Intrinsic force sensing for motion estimation in a parallel, fluidic soft robot for endoluminal interventions

Lukas Lindenroth*, Jeref Merlin, Sophia Bano, Joseph G. Manjaly, Nishchay Mehta and Danail Stoyanov

***Abstract*—Determining the externally-induced motion of a soft robot in minimally-invasive procedures is highly challenging and commonly demands specific tools and dedicated sensors. Intrinsic force sensing paired with a model describing the robot's compliance offers an alternative pathway which relies heavily on knowledge of the characteristic mechanical behaviour of the investigated system. In this work, we apply quasi-static intrinsic force sensing to a miniature, parallel soft robot designed for endoluminal ear interventions. We characterize the soft robot's nonlinear mechanical behaviour and devise methods for inferring forces applied to the actuators of the robot from fluid pressure and volume information of the working fluid. We demonstrate that it is possible to detect the presence of an external contact acting on the soft robot's actuators, infer the applied reaction force with an accuracy of 28.1mN and extrapolate from individual actuator force sensing to determining forces acting on the combined parallel soft robot when it is deployed in a lumen, which can be achieved with an accuracy of 75.45mN for external forces and 0.47Nmm for external torques. The intrinsically-sensed external forces can be employed to estimate the induced motion of the soft robot in response to these forces with an accuracy of 0.11mm in translation and 2.47° in rotational deflection. The derived methodologies could enable designs for more perceptive endoscopic systems and pave the way for developing sensing and control strategies in endoluminal and transluminal soft robots.**

***Index Terms*—Soft robotics applications, Medical Robots and Systems, Computer Vision for Medical Robotics**

I. Introduction

SOFT robots provide the inherent advantage of being able to conform with their environment. This opens up new pathways in clinical interventional and surgical procedures, particularly for endoluminal or transluminal approaches where robots and surgical tools have to be highly adaptable to the patient anatomy. For delicate surgical scenarios, the compliance and softness of such robots can pose significant challenges, which is further augmented when a human operator in the loop interacts with the device.

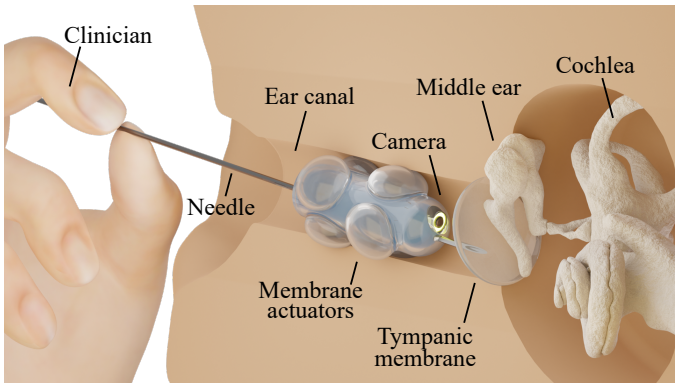

Fig. 1: Overview of the envisioned soft robot for guidance during intratympanic steroid injections.

In our previous work we have introduced the design of a fluid-driven endoluminal soft robot with the potential to aid needle guidance through the ear canal when delivering intratympanic injections [1]. An overview of the soft robot-assisted workflow is shown in Fig. 1. Such injections are the first-in-line treatment for sudden sensorineural hearing loss and Meniere's disease [2], [3] and are commonly administered by trained ear, nose and throat (ENT) surgeons. During the envisioned soft robot-assisted procedure, which is depicted in Fig. 2, the robot anchors itself in the surrounding ear canal (Fig. 2a)) while the needle is introduced through a guide channel close to the robot's centre. The guide is steered towards the desired point of needle insertion on the tympanic membrane with the help of radially-aligned fluidic actuators (Fig. 2b)). The desired insertion point can be identified with the help of an on-board endoscopic camera. Once positioned, the robot provides a straight trajectory to the target insertion point. During the insertion of the needle the robot is able to passively suppress undesired, minor and involuntarily-induced motion at the proximal end of the needle by the operating clinician as part of the procedure (Fig. 2c)) [1]. This is achieved by the mechanical elastic coupling between robot and surrounding lumen. Larger motions which are not suppressed by the morphology of the system on the other hand may considerably deflect the robot from its alignment with the desired needle trajectory, which could pose severe risks to the patient, as damaging the surrounding ear anatomy could result in permanent hearing loss for the patient. Therefore, means to detect or predict such events could be greatly beneficial in facilitating pathways for the clinical adoption of the prescribed technology.

A variety of feedback mechanisms could be employed to sense potential deflection of the soft robot. Estimating ego-

Manuscript received: Feb., 25, 2022; Revised June, 1, 2022; Accepted July, 19, 2022.

This paper was recommended for publication by Editor Yong-Lae Park upon evaluation of the Associate Editor and Reviewers' comments.

*This research was funded in whole, or in part, by the Wellcome/EPSRC Centre for Interventional and Surgical Sciences (WEISS) [203145/Z/16/Z]; the Engineering and Physical Sciences Research Council (EPSRC) [EP/P027938/1, EP/R004080/1, EP/P012841/1]; and the Royal Academy of Engineering Chair in Emerging Technologies Scheme [CiET1819/2/36]. For the purpose of open access, the author has applied a CC BY public copyright licence to any author accepted manuscript version arising from this submission.

L. Lindenroth, J. Merlin, S. Bano and D. Stoyanov are with the Wellcome/EPSRC Centre for Interventional and Surgical Sciences (WEISS), University College London, 43-45 Foley St., Fitzrovia, London W1W 7EJ, UK

J. G. Manjaly and N. Mehta is with the University College London Hospitals Biomedical Research Centre, National Institute for Health Research, London, UK and the Royal National ENT & Eastman Dental Hospitals, University College London Hospitals, UK

Corresponding author: Lukas Lindenroth (l.lindenroth@ucl.ac.uk)

Digital Object Identifier (DOI): see top of this page.

This article has been accepted for publication in IEEE Robotics and Automation Letters. This is the author's version which has not been fully edited and content may change prior to final publication. Citation information: DOI 10.1109/LRA.2022.3193627

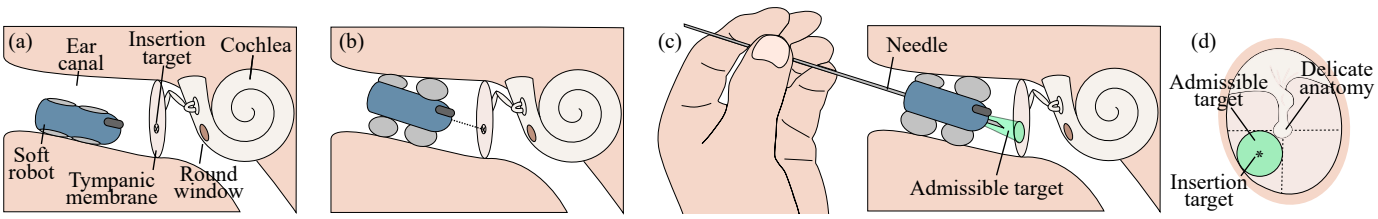

Fig. 2: Overview of the soft robot-guided needle insertion procedure. The deflated soft robot is manually positioned in the ear canal (a) and inflated to establish contact with the surrounding lumen. Once deployed, the membrane actuators are differentially driven to align the robot's needle guide with the anatomical target on the tympanic membrane (b). Upon reaching the desired target, the human operator inserts the needle which is guided to the desired target (c). If deflection of the needle occurs prior to insertion, a maximum deflection from the target on the tympanic membrane can be defined (admissible target), which ensures that the needle is inserted in the appropriate location away from delicate anatomy (d).

motion in endoscopy for example shows promising results in image-guided control [4]. Vision-based methods tend to work well in good contrasted, textured scenes captured from a high resolution camera, having repetitive features, trackable across consecutive frames. However, motion estimation in endoscopy, especially from a miniature camera mounted on a soft endoluminal interventional robot, inherently poses various challenges due to poor resolution, low illumination and spotlight light source and texture paucity. Additionally, motion estimation at high rates is commonly limited by the bandwidth of the employed camera and dependent on the computational complexity of the algorithm. These challenges currently limit vision-based motion estimation in miniature surgical robotic systems, where accurate and real-time estimation is required. Force sensing, on the other hand, may help in reliably inferring needle motion at a much higher rate.

Due to the size constraints imposed by the application, integrating dedicated sensors into the robotic system is difficult. Intrinsically sensing forces or wrenches applied to a robotic device without dedicated force-torque sensors is common practice in traditional rigid robotic systems [5], [6]. More recently, with the drive towards flexible surgical tools and continuum robotic devices, research efforts have been expanded towards intrinsic force sensing in continuum and parallel continuum robots [7], [8]. Doing so in the context of fluid-driven soft robots, however, poses additional challenges due to the highly nonlinear mechanical properties of the employed materials, fluid actuator dynamics, as well as the inherent underactuation associated with soft devices. We have previously attempted to address this by estimating contact forces applied at the tip of a hydraulic soft continuum manipulator [9], as well as by characterising the mechanical response of a three legged parallel soft robot and subsequently deducing the externally applied force [10].

Recently, fluidic membrane-based actuation has been receiving attention, both in our own works as well as from the soft robotics community [11]. Using thin silicone rubber membranes to generate motion can be highly efficient in applications requiring deployability, which is a common factor in endoluminal and transluminal procedures [12]. Despite the potential of this actuation modality, efficient modelling and control of such actuators is challenging and therefore demands further investigation [13].

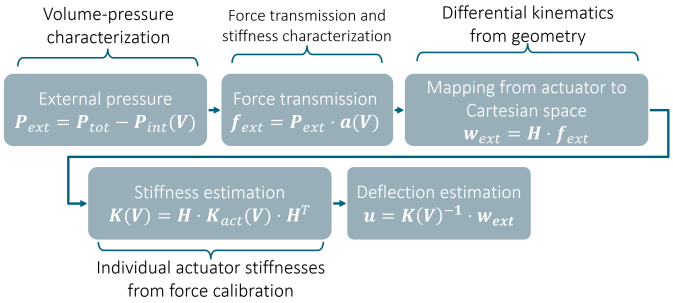

Fig. 3: Overview of the proposed deflection estimation algorithm with the respective experimental characterisations.

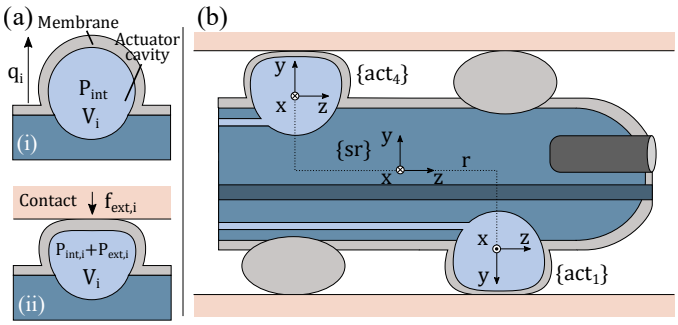

Fig. 4: Parameterization of a fluidic membrane actuator under inflation by a set fluid volume V_i with respective pressure response $P_{int,i}$ to a radial displacement of q_i unconstrained (a-i) and when a contact force $f_{ext,i}$ is applied along its primary axis of inflation (a-ii) as well as transformation from local actuator frames (e.g.$\{act_1\}$ and $\{act_4\}$) to global Cartesian frame $\{sr\}$.

This work presents a first investigation into employing quasi-static intrinsic force sensing in a deployable, endoluminal soft robot [1] with the aim to determine the deflection of the latter under an external load without the need for dedicated sensors. For this purpose we adapt paradigms derived in our previous work for a soft ultrasound robot end-effector [10]. The soft robot investigated here employs a drastically different form of actuation, namely fluidic membranes, to achieve motion, which exhibit substantially more nonlinear behaviour than the fluid actuators investigated in [10]. The design requires contact to be established between soft robot and environment, hence we demonstrate that contact estimation be-

This article has been accepted for publication in IEEE Robotics and Automation Letters. This is the author's version which has not been fully edited and content may change prior to final publication. Citation information: DOI 10.1109/LRA.2022.3193627

tween individual actuators and the lumen surrounding the soft robot is feasible. The work significantly expands our previous research by not only enabling prediction of applied forces but now also torques and employing the intrinsically-sensed forces and torques to determine the soft robot deflection in real-time without the need for any dedicated force or positioning sensor. For the particular application of intratympanic steroid injections, such capabilities could greatly contribute to patient comfort and procedure outcome by indicating potentially-occurring deflection of the needle, which could in return lead to misalignment of the needle prior to insertion or stress build-up in the tympanic membrane thereafter. Estimation of the robot's deflection from intrinsically-sensed forces and torques is achieved by characterising the robot's active inflation behaviour as well as its mechanical response to external loading. A formulation is derived to relate internal fluid pressure variation under a given fluid volume to external contacts and forces applied to individual actuators, as well as the combined parallel soft robot under consideration of the highly nonlinear characteristics of the system. Together with the combined stiffness of the soft robot, the intrinsically-sensed force is then applied to compute the soft robot's deflection under the external load.

II. Methods

In the following sections, methodologies to first determine the external force applied to the soft robot and its resulting motion are deduced. The state of the robot is defined by the fluid actuator volume $\boldsymbol{V}$ and the measured fluid pressure $\boldsymbol{P}$. According to these quantities, the external force and soft robot motion are derived. An overview of the proposed methodology is shown in Fig. 3

A. Preliminaries

The utilised parallel soft robot design has first been introduced in our previous work [1]. It consists of a cylindrical body with a hard silicone rubber core (Smooth-Sil 960, Smooth-On Inc., Macungie, PA, US) covered by a softer silicone rubber membrane (Ecoflex 00-30, Smooth-On Inc., Macungie, PA, US). Six fluidic actuators are created through dome-shaped cavities in the harder core which, under fluidic pressurisation, allow for inflating the covering membrane and thus generate radial motion. As shown in our previous work, the soft robot is able to generate motion primarily in four degrees-of-freedom, namely translation and rotation normal to its long-axis. This is achieved by inducing differential actuator motion.

The differential kinematics of the soft robot can be employed to relate individual actuator motions to the overall soft robot motion and similarly map actuator forces and torques to combined wrenches acting on the robot as a whole. The actuator space of the system is defined by the local actuation variables of the soft robot (namely fluid volume $\boldsymbol{V} \in [6 \times 1]$ and fluid pressure $\boldsymbol{P} \in [6 \times 1]$) acting in their respective frames $\{act_i\}$ as shown in Fig. 4. The Cartesian space, often referred to as Task space, is comprised of the global state of the soft robot (its pose change $\boldsymbol{u} = [d_x, d_y, \theta_x, \theta_y]^T$ and the global wrench acting in its centre $\boldsymbol{w}_{ext} = [f_x, f_y, t_x, t_y]^T$) and is denoted as $\{sr\}$. The mapping between the two spaces can be achieved with the help of the inverse Jacobian matrix $\boldsymbol{J}^{-1}$, or actuation matrix $\boldsymbol{H} = \boldsymbol{J}^{-T}$, such that

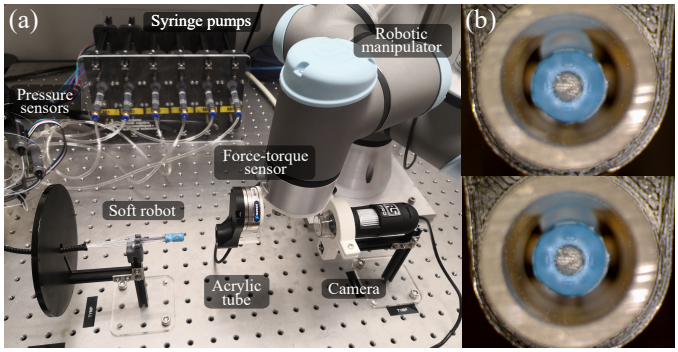

Fig. 5: Experimental setup for intrinsic force sensing validation (a) and exemplary front view of soft robot with actuator under compression (b).

$$\boldsymbol{w}_{ext} = \boldsymbol{H} \cdot \boldsymbol{f}_{ext} \tag{1}$$

and

$$\boldsymbol{q} = \boldsymbol{H}^T \cdot \boldsymbol{u} \tag{2}$$

Where $\boldsymbol{q} = [q_1, q_2, ..., q_n]^T$ are axial actuator displacements and $\boldsymbol{f}_{ext} = [f_1, f_2, ..., f_n]^T$ are the respective external forces acting on the n actuators. In our previous work [1] (Eqs. (1-4)) we have derived the soft robot's actuation matrix $\boldsymbol{H} \in [4 \times 6]$ according to the individual actuator forces which are radially applied to the lumen walls and their respective adjoint transformations relative to the frame of the soft robot, in a similar manner as previously shown for our design for a soft ultrasound end-effector [14]. The respective mappings are indicated for $\{act_1\}$ and $\{act_4\}$ in Fig.4b). It can be defined by

$$\boldsymbol{H}^T = \boldsymbol{J}^{-1} = \begin{bmatrix} 0 & 1 & -r & 0 \\ -\frac{\sqrt{3}}{2} & -\frac{1}{2} & \frac{1}{2}r & -\frac{\sqrt{3}}{2}r \\ \frac{\sqrt{3}}{2} & -\frac{1}{2} & \frac{1}{2}r & \frac{\sqrt{3}}{2}r \\ 0 & -1 & -r & 0 \\ \frac{\sqrt{3}}{2} & \frac{1}{2} & \frac{1}{2}r & -\frac{\sqrt{3}}{2}r \\ -\frac{\sqrt{3}}{2} & \frac{1}{2} & \frac{1}{2}r & \frac{\sqrt{3}}{2}r \end{bmatrix} \tag{3}$$

where $r = 3.5$mm is the distance between the actuators and the centre of the robot. Translation along and rotation around the main axis of the robot are both ignored as the respective motions are negligible and irrelevant for the envisioned application. This formulation, which represents a mapping between Cartesian space and actuator space of the robot, can be employed to infer forces and torques applied to the robot's centre.

B. Intrinsic force sensing

To induce motion, the radial membrane actuators are inflated by a pressurized fluid of known volume $\boldsymbol{V}$. In this work, we assume that the fluid is incompressible and hence the fluid volume inside the actuator cavities can be easily inferred from the externally induced fluid volume under the assumption that expansion of the fluid tubing can be ignored. External

This article has been accepted for publication in IEEE Robotics and Automation Letters. This is the author's version which has not been fully edited and content may change prior to final publication. Citation information: DOI 10.1109/LRA.2022.3193627

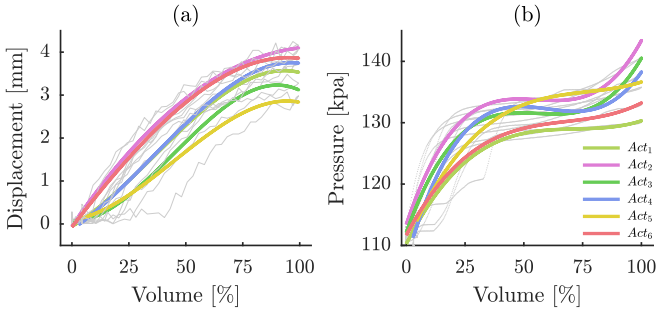

Fig. 6: Actuator inflation and pressure characterisation with the interpolated radial displacement (a) and interpolated internal pressure P_{int} (b) for each actuator during the inflation.

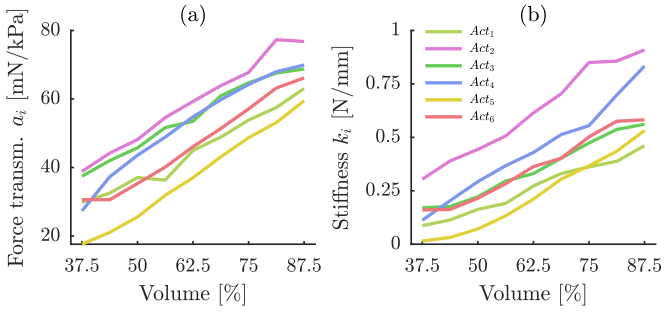

Fig. 7: Force transmission (a) and radial actuator stiffness (b) for individual actuators.

forces applied to the soft actuators are estimated from fluid pressure variations. The internal pressure inside an actuator i, $P_{int,i}$, is generated by the stretch of the actuator membrane according to the introduced fluid volume. Pressure variation generated by an external force acting on the soft actuator, $P_{ext,i}$, is a function of the force magnitude and direction as well as the initial stretch of the membrane actuator due to the highly nonlinear behaviour of the actuators. An overview of the respective quantities under actuator inflation is shown in Fig. 4. If the total fluid pressure of an actuator i is given as $P_{tot,i}$, the external pressure is defined as

$$P_{ext,i} = P_{tot,i} - P_{int,i} \tag{4}$$

As the actuators balloon radially, the contact area varies noticeably with the level of inflation of the actuator. We therefore introduce a nonlinear function $f_{ext,i}/P_{ext,i} = a_i(V_i)$ which approximates the contact area relative to the introduced fluid volume V_i for a contact area as large as or larger than the diameter of the actuator, and thus describes the force transmission between external force and pressure variation. For simplifying this relationship, it is assumed that the contact height relative to the surface of the ballooning actuator at which the force acts is constant. Similarly, internal actuator pressures $P_{int,i}$ can be defined as a nonlinear function of the induced fluid volume V_i.

The external force is mapped from individual actuator forces $f_{ext,i}$ to forces acting at the centre of the robot in Cartesian space through the previously-derived actuation matrix. The static force relationship can be written as

$$\boldsymbol{w}_{ext} = \boldsymbol{H} \cdot \boldsymbol{f}_{ext} = \boldsymbol{H} \cdot \boldsymbol{P}_{ext} \cdot \boldsymbol{a}(\boldsymbol{V}) \tag{5}$$

For a given external wrench, the force variation in actuator space can be approximated by

$$\boldsymbol{f}_{ext} = \boldsymbol{H}^{\dagger} \boldsymbol{w}_{ext} \tag{6}$$

Where $\boldsymbol{H}^{\dagger}$ denotes the Moore–Penrose inverse of the actuation matrix.

C. Motion estimation

The previously-derived methodology for intrinsically sensing an external force applied to the soft robot can now be employed to estimate its resulting passive motion. The motion of the soft robot within the constraint of the surrounding lumen caused by an external force can be predicted by assuming quasi-static behaviour through determining its stiffness, which relates its local motion $\boldsymbol{u}$ to an external wrench $\boldsymbol{w}_{ext}$ acting on it. This can be written as

$$\boldsymbol{w}_{ext} = \boldsymbol{K}(\boldsymbol{V}) \cdot \boldsymbol{u} \tag{7}$$

Where $\boldsymbol{K}(\boldsymbol{V})$ is the stiffness matrix of the soft robot in Cartesian space for a given fluid volume configuration $\boldsymbol{V}$. Given the previously-derived equalities, $\boldsymbol{q} = \boldsymbol{H}^T \cdot \boldsymbol{u}$ and $\boldsymbol{w}_{ext} = \boldsymbol{H} \cdot \boldsymbol{f}_{ext}$ it can be simply shown that [15]

$$\boldsymbol{K}(\boldsymbol{V}) = \boldsymbol{H} \cdot \boldsymbol{K}_{act} \cdot \boldsymbol{H}^T = \boldsymbol{H} \cdot \begin{bmatrix} k_1(V_1) & & \\ & \ddots & \\ & & k_{n(V_n)} \end{bmatrix} \cdot \boldsymbol{H}^T \tag{8}$$

Where $\boldsymbol{K}_{act} = diag(k_1, k_2, ..., k_n)$ is composed of the individual actuator stiffnesses k_i along their respective direction of motion in the local actuator frames $\{act_i\}$ for given inflation volumes V_i.

The resulting deflection $\boldsymbol{u}$ of the soft robot can then be written as

$$\boldsymbol{u} = \boldsymbol{K}(\boldsymbol{V})^{-1} \cdot \boldsymbol{w}_{ext} \tag{9}$$

D. Experimental evaluation

The soft robot is actuated through a set of stepper motor-driven hydraulic syringe pumps which are controlled by a motion controller (TMCM-6214, Trinamic GmbH, Germany). The fluid tubing is equipped with pressure sensors (MPRLS0025PA, Honeywell, United States) with a maximum pressure of 172kPa. The sensors are introduced into the fluid system through custom 3d-printed connectors. Sensor readings are compiled by a microcontroller (Teensy 4.0, PJRC, Sherwood, USA) and streamed to a laptop running ROS. The force sensing and motion estimation approaches are validated by firstly characterising mechanical responses of the individual actuators, validating the force sensing capabilities of individual actuators and subsequently the overall soft robot. An overview of the validation setup is shown in Fig. 5.

The actuators are characterised in an inflation-deflation sequence across the maximum fluid volume (0.76ml). Actuator inflation distances are tracked visually through an optical microscope placed along the main axis of the the soft robot while internal pressures $\boldsymbol{P}_{int}$ are monitored with the inline fluid pressure sensors.

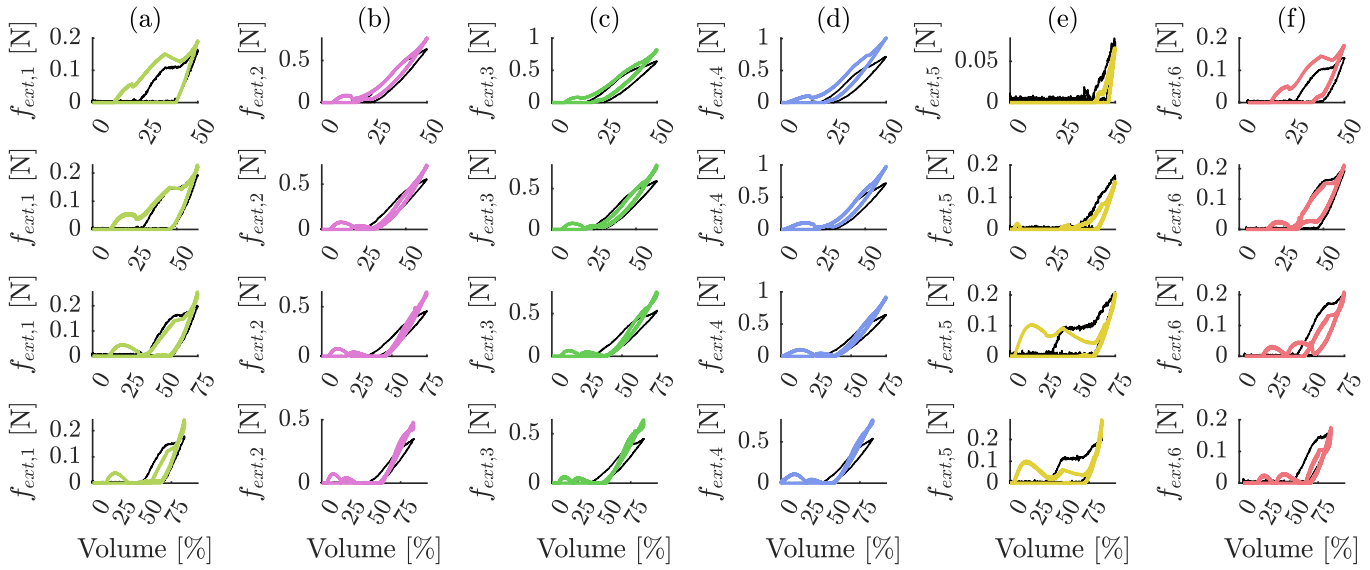

Fig. 8: Results of contact and force estimation for all six actuators (a-f) at 0.5mm, 1mm, 1.5mm and 2mm distance from the soft robot surface (top to bottom) indicating the external force as a function of the introduced fluid volume where the black line indicates the measured reference.

The actuators' responses to external forces are determined by inducing radial displacements with an acrylic tube (ID 14mm) which is mounted via a force-torque sensor (Mini40, ATI Industrial Automation, NC, USA) to the tip of a robotic manipulator (UR3, Universal Robots, Odense, Denmark). The soft robot is mechanically fixed in space. The acrylic tube is aligned parallel to the main axis of the soft robot. Fluid pressure and force responses are monitored by the inline pressure sensors and the force-torque sensor respectively for varying fluid volumes. Contact estimation and intrinsic force sensing for individual actuators are validated by gradually inflating and deflating individual actuators against the acrylic tube which is positioned at different radial distances to the soft robot.

Intrinsic force sensing and ego-motion in Cartesian space are validated by inflating the soft robot such that the actuators are sufficiently expanded to interact with the surrounding, centered lumen, which equates to approximately 75% to 87.5% of inflation volume. The robotic manipulator is moved in arbitrary directions in the plane orthogonal to the main axis of the soft robot while retaining its orientation with forces in the range of 1N and displacements of approximately 1mm. Similarly, the surrounding lumen is tilted in the range of approximately $\pm 15°$ around the soft robot's x- and y-axis.

Assuming a circular target of the tilted tympanic membrane with a diameter of 7mm [16], the admissible target will have a radius of 1.45mm such as shown in Fig 2d). Since the average length of the human ear canal is 25mm [16], assuming that the robot is placed in the middle of the ear canal, the total deflection induced by the combination of translational and rotational errors should not exceed 1.45mm to avoid harming the surrounding delicate anatomy.

III. Results

A. Actuator inflation characterisation

Results for individual actuator characterizations are presented in Fig. 6. Radial endpoints of the membrane actuators are tracked manually on the respective images. The corresponding radial displacements are presented in Fig. 6a), ranging from a maximum inflation of 3.07mm for actuator 5 to 4.25mm for actuator 2. Pressure responses induced by the expanding actuator membranes for increasing fluid volumes are shown in Fig. 6b). Maximum pressures range from 129.97kPa for actuator 1 to 140.66kPa for actuator 2. The pressure response as a function of the introduced fluid volume is described as a 3rd-order polynomial, which is fitted to the experimental data.

B. Actuator force response

The actuators' responses to external loading are presented in Fig. 7. Both the force transmission and stiffness responses are evaluated for fluid volumes ranging from 37.5% to 87.5% of the maximum inflation to minimize the highly nonlinear inflation behaviour of the membrane for small inflation volumes. The force transmission, relating the internal fluid pressure variation to an external force measured by the force-torque sensor is characterized for compression resulting in forces between 0 and 0.5N. The force transmission $a_i(V_i)$ (shown in Fig. 7a)) is mapped by linearizing the force-pressure response at a given fluid volume V_i. It varies substantially across fluid volumes and actuators with a minimum of approximately 17.61mN/kPa for actuator 5 to a maximum of 77.32mN/kPa for actuator 2 and a mean force transmission of 49.25±14.57mN/kPa. Actuator stiffnesses are presented in Fig. 7b), ranging from a minimum of 0.02N/mm for actuator 5 to 0.92N/mm for actuator 2 with a mean actuator stiffness of 0.38 ± 0.04N/mm across all actuators and inflation levels.

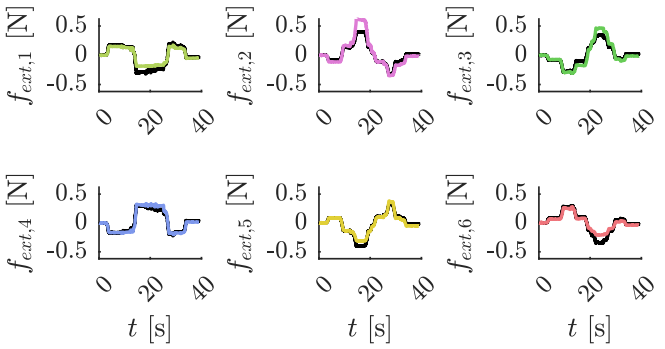

Fig. 9: Actuator force variation in a single trial with the individual actuator forces decomposed from the force measurement for a trajectory in Cartesian space where the black line indicates the measured reference.

C. Contact and force sensing in actuator space

Results for contact estimation and respective force sensing are shown in Fig. 8. The distance between soft robot and contact provided by the acrylic tube is varied from 0.5mm in 0.5mm increments to 2mm, leading to a total of four trajectories for each actuator. The corresponding maximum inflation volume to reach the contact is varied from 37.5% inflation in 12.5% increments to 87.5% inflation according to the defined contact distance to avoid over-pressurizing the actuators.

Contact estimation is evaluated by determining the number of samples for at which the contact estimate $c_i(f_{ext,i})$ is correctly predicted such that

$$c_i(f_{ext,i}) = \begin{cases} 1, & \text{if } f_{ext,i} > 0mN. \\ 0, & \text{otherwise.} \end{cases} \tag{10}$$

For the evaluated trajectories contact is on average predicted 83.26% of the sampling time with wrongly-predicted contact more prominently occurring for higher fluid volumes. The algorithm is commonly overestimating the contact condition, particularly in case of the dynamic peaks occurring at the beginning and end of the inflation sequences, noticeable primarily for r $\geq$1mm.

The accuracy between contact force measurement and prediction varies significantly across actuators. It can be seen that the prediction shown in Fig. 8 tracks the trend of the external force well, with an average error of 28.1 ± 38.8mN across all actuators and distances. The largest errors appear in actuator 4 with a maximum error of 299mN at a peak force of 716.9mN. The mean errors across actuators are 6.98%, 6.34%, 7.32%, 8.65%, 9.42% and 7.59% for actuators 1-6 respectively, normalized to the maximum measured force value for each timeseries. Taking into account the mean stiffness across all actuators of 0.38N/mm, and as such the mean compliance of 2.64mm/N, the average force error leads for a single actuator to a deflection estimation error of 0.074$\pm$0.1mm.

D. Force sensing and motion estimation in Cartesian space

Intrinsic force sensing in Cartesian space is validated by inducing relative movement between soft robot and surrounding acrylic tube while measuring the reaction force. This

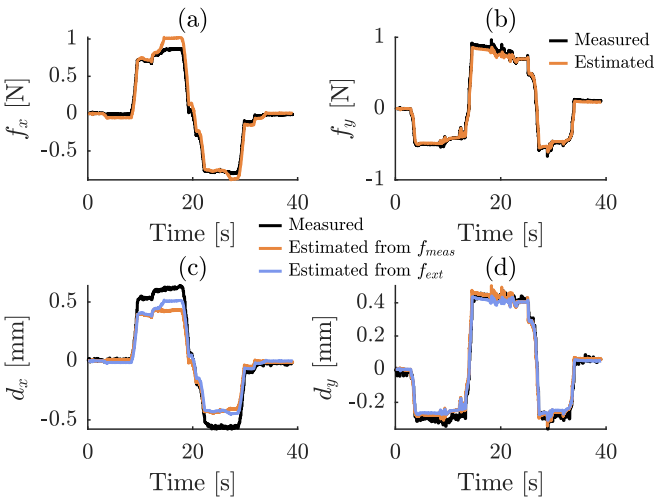

Fig. 10: Intrinsically-sensed directional forces f_x (a) and f_y (b) and resulting translational deflections d_x (c) and d_y d) induced from a defined translation of the soft robot.

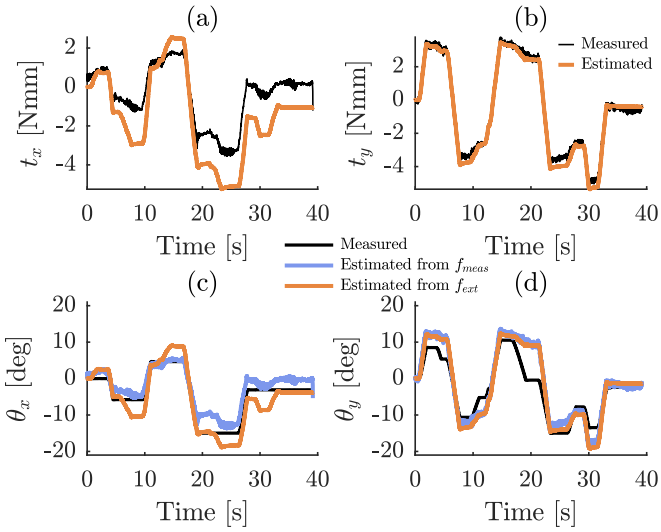

Fig. 11: Intrinsically-sensed directional torques t_x (a) and t_y (b) and resulting rotational deflections θ_x (c) and θ_y d) induced from a defined rotational deflection of the soft robot

is repeated six times, with the resulting directional forces f_x and f_y being shown in Figs. 10a) and b). The expected corresponding local forces acting on the individual actuators are computed from the measured force according to Eq. (6) and are shown in Fig. 9.

The resulting mean absolute errors and standard deviations between measured and estimated forces are presented in Fig. 12a). Errors in f_y are with an average of 64.8mN lower compared to errors in f_x with 86.1mN. Across trials the force error follows a similar trend reaching a minimum of 50.6 ± 66.56mN in f_x and 24.12 ± 34.8mN in f_y for trial 4 and a maximum 122.23 ± 144.91mN in f_x and 115.87 ± 134.81mN in f_y across trials.

The results of the motion estimation are presented in Fig. 10c) and d) for a single timeseries and in Fig. 13 indicating errors in d_x and d_y across all trials for deflections estimated from the force sensor readings (a) and from the intrinsic force

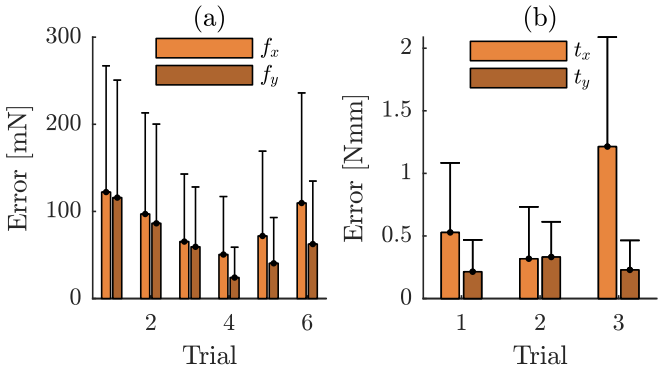

Fig. 12: Mean absolute errors for sensing directional forces across six trials (a) and torques across three trials (b)

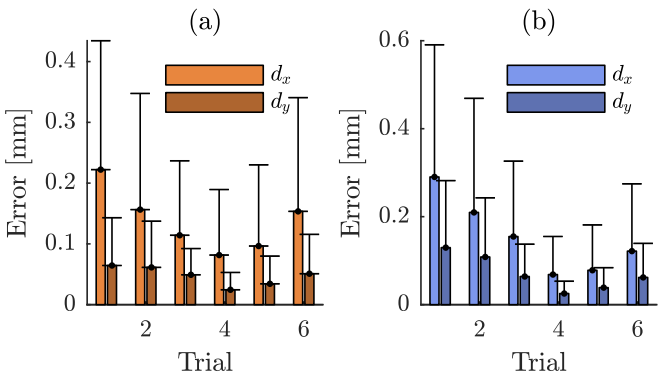

Fig. 13: Errors in estimated motion d_x and d_y across six trials from measured forces (a) and estimated forces (b)

sensing capabilities of the robot (b). Mean absolute errors and respective standard deviations for motion estimations in x and y directions based on the measured force are shown in Fig. 13a) whilst motion estimated from the intrinsically-sensed force is presented in Fig. 13b), which follow a similar trend compared to the sole force estimation results with deflection errors ranging from 0.025mm in d_y to 0.29mm in d_x, both for motion estimated from the intrinsically-sensed external force. Therefore, the mean deflection error from estimated forces is 0.11±0.13mm across both d_x and d_y. Torques and resulting rotations are induced similarly by applying a defined rotational deflection to the soft robot. This is repeated for three trajectories, of which one is presented in Fig. 11. The resulting error in intrinsic torque sensing is presented in Fig. 12b). It is noticeable that, in some occasions, despite the enforced rotation of the robot the resulting torque is not affected (Fig. 11d), e.g. at 18s), which could be the result of slippage between soft robot and surrounding lumen. It can be seen that the torques can be intrinsically sensed with an accuracy of 0.47±0.44Nmm. An overview of the deflection estimation results across all trials is shown in Fig. 14. The resulting mean deflection estimation in rotation is 2.47±2.73°, with substantially greater errors occurring in the $y-$ than in the $x-$direction, which is in-line with the translation estimation findings.

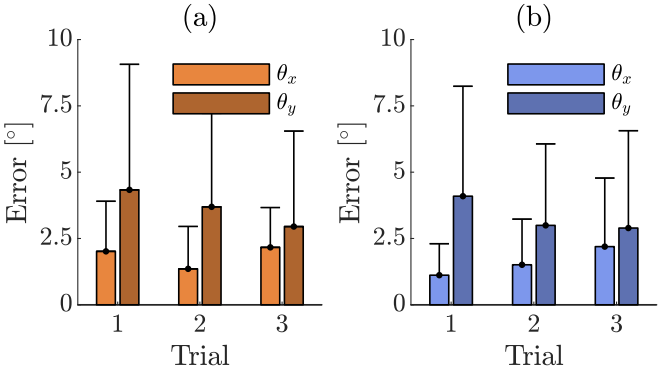

Fig. 14: Errors in estimated rotation θ_x and θ_y across three trials from measured torques (a) and estimated torques (b)

IV. Discussion

The mechanical characterization of the membrane actuators indicates significant variation across actuators in radial inflation and subsequently pressure, force transmission and stiffness. Particularly due to the small scale of the system, a number of factors potentially contribute to this variability. Small variations in the diameter of the membrane actuator, such as minor detachment of the soft membrane from the harder rubber core, could lead to substantial pressure variation. Air entrapped in the fluid system can also have a profound impact on the inflation characteristics, which in return impacts the actuators' other mechanical properties. The force transmission, which is directly linked to the force sensing sensitivity, varies substantially across the investigated fluid volume range (in case of actuator 5 the transmission triples with the decreasing fluid volume). Whilst it has been shown that intrinsic force sensing is feasible in the proposed system, accurate calibration is of paramount importance for successful force estimation.

It can be seen that whilst the contact and force estimation accuracy is similar across actuators when performed individually, the accuracy of estimating forces in Cartesian space is greatly impacted by the force direction. In x-direction of the robot the force measurement error is significantly greater compared to the y-direction. The unmodelled deformation behaviour of the actuators due to non-radial forces could be one of the contributors to this behaviour.

Determining the force transmission to enable accurate force sensing is difficult, particularly when the surrounding anatomy is irregular and unknown. To address this, the design of the soft robot could be adapted to ensure a more consistent contact point between soft robot and the surrounding lumen. This could be achieved by locally altering the composition of the membrane in a defined region, e.g. through reinforcements or deposition of harder silicone rubber, and thus creating a known contact interface. Alternatively, a combination of sensing and modelling could be employed to describe the inflation profile of the membrane actuator and subsequently determine the contact area.

Due to the design of the soft robot, forces acting along or torques applied around the main longitudinal axis of the robot are omitted due to the manual insertion of the needle and

therefore shearing forces leading to sliding of the membrane actuators relative to the surrounding lumen are unlikely occur. Despite that, we have observed increased sensing and deflection estimation errors when a rotational deflection is induced, which could be a result of contact delamination. Modelling friction effects could therefore be a way to further improve estimation accuracy.

The work provides a first step towards more perceptive, fluid-actuated, deployable endoluminal or transluminal medical devices and could find application across a number of clinical specialties and applications which are targeted to be addressed with the help of fluid-driven soft robotics technologies, such as intra-body mechano-stimulation of tissues [12], [17], colonoscopy [18], [19] or wider endoscopic interventions [20].

V. Conclusion

This work has demonstrated that a present contact applied to the soft robot's ballooning actuators can be inferred and the resulting contact force estimated with an average accuracy of 28.1 ± 38.8mN. The measured actuator forces allow determining the force acting in Cartesian space on the robot body. Directional forces and torques can be predicted with an accuracy of 75.45mN and 0.47Nmm respectively. The intrinsically-sensed forces and torques allow estimating the resulting passive motion of the robot with an accuracy of 0.11 ± 0.13mm in translation and $2.47 \pm 2.73^\circ$ in rotation. Based on the combination of translational and rotational errors, the average total deflection error is found to be 0.54mm with the maximum deflection error of 1.14mm. Since the maximum total deflection error is smaller than the radius of the admissible target of the ear drum, this shows that the deflection estimation method could be successfully employed to determine potentially unsafe deflection of the needle. The capabilities provided by intrinsic force sensing and resulting motion estimation could help in creating more interactive soft robots. Measuring forces inside a natural orifice when performing an intervention endoluminally or transluminally could provide intraoperative feedback which could enhance the operator's perception, serve as a safety metric for developing more autonomous robotic control or aid in assessing operator performance for training purposes as well as procedure outcomes.

References

[1] L. Lindenroth, S. Bano, A. Stilli, J. G. Manjaly, and D. Stoyanov, "A Fluidic Soft Robot for Needle Guidance and Motion Compensation in Intratympanic Steroid Injections," IEEE Robotics and Automation Letters, vol. 6, no. 2, pp. 871–878, 4 2021.

[2] M. Patel, K. Agarwal, Q. Arshad, M. Hariri, P. Rea, B. M. Seemungal, J. F. Golding, J. P. Harcourt, and A. M. Bronstein, "Intratympanic methylprednisolone versus gentamicin in patients with unilateral Ménière's disease: a randomised, double-blind, comparative effectiveness trial," The Lancet, vol. 388, no. 10061, pp. 2753–2762, 2016. [Online]. Available: http://dx.doi.org/10.1016/S0140-6736(16)31461-1

[3] M. Lechner, L. Sutton, M. Ferguson, Y. Abbas, J. Sandhu, and A. Shaida, "Intratympanic Steroid Use for Sudden Sensorineural Hearing Loss: Current Otolaryngology Practice," Annals of Otology, Rhinology and Laryngology, vol. 128, no. 6, pp. 490–502, 2019.

[4] Z. Zhang, B. Rosa, O. Caravaca-Mora, P. Zanne, M. J. Gora, and F. Nageotte, "Image-Guided Control of an Endoscopic Robot for OCT Path Scanning," IEEE Robotics and Automation Letters, vol. 6, no. 3, pp. 5881–5888, 2021.

[5] K. Ohishi, M. Miyazaki, M. Fujita, and Y. Ogino, "Hybrid Control of Robot Manipulator without Force Sensor," IFAC Proceedings Volumes, vol. 26, no. 2, pp. 991–996, 1993. [Online]. Available: http://dx.doi.org/10.1016/S1474-6670(17)48619-8

[6] K. S. Eom, I. H. Suh, W. K. Chung, and S. R. Oh, "Disturbance observer based force control of robot manipulator without force sensor," Proceedings - IEEE International Conference on Robotics and Automation, vol. 4, no. May, pp. 3012–3017, 1998.

[7] K. Xu and N. Simaan, "An investigation of the intrinsic force sensing capabilities of continuum robots," IEEE Transactions on Robotics, vol. 24, no. 3, pp. 576–587, 2008.

[8] R. Roy, L. Wang, and N. Simaan, "Investigation of effects of dynamics on intrinsic wrench sensing in continuum robots," Proceedings - IEEE International Conference on Robotics and Automation, vol. 2016-June, pp. 2052–2059, 2016.

[9] L. Lindenroth, C. Duriez, J. Back, K. Rhode, and H. Liu, "Intrinsic force sensing capabilities in compliant robots comprising hydraulic actuation," in IEEE International Conference on Intelligent Robots and Systems, vol. 2017-Septe, 2017, pp. 2923–2928.

[10] L. Lindenroth, D. Stoyanov, K. Rhode, and H. Liu, "Towards intrinsic force sensing and control in parallel soft robots," Transaction on Mechatronics, 2022. [Online]. Available: http://arxiv.org/abs/2111.10338

[11] R. H. Osgouei, L. Marechal, C. Kontovounisios, and F. Bello, "Soft Pneumatic Actuator for Rendering Anal Sphincter Tone," IEEE Transactions on Haptics, vol. 13, no. 1, pp. 183–190, 2020.

[12] E. Perez-Guagnelli, J. Jones, and D. D. Damian, "Hyperelastic Membrane Actuators: Analysis of Toroidal and Helical Multifunctional Configurations," Cyborg and Bionic Systems, vol. 2022, 2022.

[13] N. Herzig, J. Jones, E. Perez-Guagnelli, and D. D. Damian, "Model and Validation of a Highly Extensible and Tough Actuator based on a Ballooning Membrane," no. Icra, pp. 11 961–11 967, 2021.

[14] L. Lindenroth, R. J. Housden, S. Wang, J. Back, K. Rhode, and H. Liu, "Design and integration of a parallel, soft robotic end-effector for extra-corporeal ultrasound," IEEE Transactions on Biomedical Engineering, pp. 1–1, 12 2019.

[15] A. Klimchik, D. Chablat, and A. Pashkevich, "Stiffness modeling for perfect and non-perfect parallel manipulators under internal and external loadings," Mechanism and Machine Theory, vol. 79, pp. 1–28, 2014. [Online]. Available: http://dx.doi.org/10.1016/j.mechmachtheory.2014.04.002

[16] B. T. Faddis, "Structural and functional anatomy of the outer and middle ear," Anatomy and Physiology of Hearing for Audiologists, pp. 93–108, 2008.

[17] N. Herzig, J. Jones, E. Perez-Guagnelli, and D. D. Damian, "Model and Validation of a Highly Extensible and Tough Actuator based on a Ballooning Membrane," no. Icra, pp. 11 961–11 967, 2021.

[18] M. McCandless, A. Gerald, A. Carroll, H. Aihara, and S. Russo, "A Soft Robotic Sleeve for Safer Colonoscopy Procedures," IEEE Robotics and Automation Letters, vol. 6, no. 3, pp. 5292–5299, 2021.

[19] V. Consumi, J. Merlin, L. Lindenroth, D. Stoyanov, and A. Stilli, "A Novel Soft Shape-shifting Robot with Track-based Locomotion for In-pipe Inspection," 2022. [Online]. Available: https://arxiv.org/abs/2202.10840

[20] T. Ranzani, S. Russo, F. Schwab, C. J. Walsh, and R. J. Wood, "Deployable stabilization mechanisms for endoscopic procedures," Proceedings - IEEE International Conference on Robotics and Automation, pp. 1125–1131, 2017.